Ex situ and in situ Magnetic Phase Synthesised Magneto-Driven Alginate Beads

Udara Bimendra Gunatilake [a,b], Munuswamy Venkatesan [c], Lourdes Basabe-Desmonts [b,d,e,f,*], Fernando Benito-Lopez [a,d,e,*]

[a] Microfluidics Cluster UPV/EHU, Analytical Microsystems & Materials for Lab-on-a-Chip (AMMa-LOAC) Group, Analytical Chemistry Department, University of the Basque Country UPV/EHU, Spain
[b] Microfluidics Cluster UPV/EHU, BIOMICs microfluidics Group, Lascaray Research Center, University of the Basque Country UPV/EHU, Vitoria-Gasteiz, Spain
[c] School of Physics and AMBER, Trinity College, Dublin 2, Ireland
[d] Bioaraba Health Research Institute, Microfluidics Cluster UPV/EHU, Vitoria-Gasteiz, Spain
[e] BCMaterials, Basque Center for Materials, Applications and Nanostructures, UPV/EHU Science Park, Leioa, Spain
[f] Basque Foundation of Science, IKERBASQUE, María Díaz Haroko Kalea, 3, Bilbao 48013, Spain

GRAPHICAL ABSTRACT
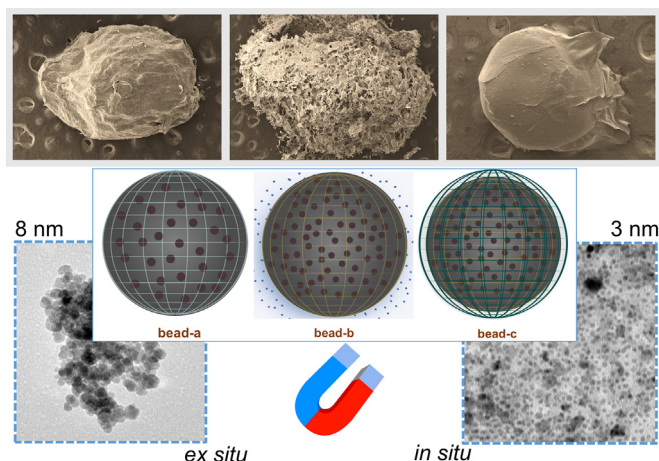
ARTICLE INFO

ABSTRACT

Biocompatible magnetic hydrogels provide a great source of synthetic materials, which facilitate remote stimuli, enabling safer biological and environmental applications. Prominently, the *ex situ* and *in situ* magnetic phase integration is used to fabricate magneto-driven hydrogels, exhibiting varied behaviours in aqueous media. Therefore, it is essential to understand their physicochemical properties to target the best material for each application. In this investigation, three different types of magnetic alginate beads were synthesised. First, by direct, *ex situ*, calcium chloride gelation of a mixture of Fe_3O_4 nanoparticles with an alginate solution. Second, by *in situ* synthesis of Fe_3O_4 nanoparticles inside of the alginate beads and third, by adding an extra protection alginate layer on the *in situ* synthesised Fe_3O_4 nanoparticles algi- nate beads. The three types of magnetic beads were chemically and magnetically characterised. It was found that they exhibited particular stability to different pH and ionic strength conditions in aqueous

* Corresponding authors at: Microfluidics Cluster UPV/EHU, Analytical Microsystems & Materials for Lab-on-a-Chip (AMMa-LOAC) Group, Analytical Chemistry Department, University of the Basque Country UPV/EHU, Spain. (Fernando Benito-Lopez); Microfluidics Cluster UPV/EHU, BIOMICs microfluidics Group, Lascaray Research Center, University of the Basque Country UPV/EHU, Vitoria-Gasteiz, Spain. (Lourdes Basabe-Desmonts).

E-mail addresses: lourdes.basabe@ehu.eus (L. Basabe-Desmonts), fernando.benito@ehu.eus (F. Benito-Lopez).

Magnetic materials
Magnetite

solution. These are essential properties to be controlled when used for magneto-driven applications such as targeted drug delivery and water purification. Therefore, this fundamental study will direct the path to the selection of the best magnetic bead synthesis protocol according to the defined magneto-driven application.

1. Introduction

Alginates are colloidal polysaccharides isolated from brown algae, which is abundant in coastal waters [1]. They are linear copolymers containing D-mannuronic acid and -L-guluronic acid residues covalently linked together in different configurations [2]. Alginates cross-link with multivalent metal ions (*e.g.* Ca^{2+}, Ba^{2+}) [3] following the "egg-box" model, which keeps the polymer as a three dimensional gelling material [4]. They are very versatile materials which are currently used for applications like delivery of low molecular weight drugs [2,5–7] and proteins [8–10], wound dressing [11–14], tissue engineering [15–16], food industry, [17–18] removal of water pollutants/heavy metals [19–20], among others [13,21].

Magnetic alginate nanocomposites are attracting attention because of their excellent biocompatibility and the possibility of remote stimuli manipulation [22–23]. When considering their magnetic properties, the inorganic magnetic phase is usually a metal oxide of Fe, Co, Ni, which is introduced into the polymer matrix [24]. These magneto-driven alginate nanocomposites have been applied for biomedical applications like targeted drug delivery, magnetic triggering drug release, enzyme immobilisation and magnetic hyperthermia [25–29]. Moreover, they have been employed for environmental applications like the magnetic removal of heavy metals, organic contaminants and dyes from water [30–32]. Interestingly, magnetic alginate nanocomposites microstructures have been fabricated and applied as magnetic actuators as micro-helical capsule robots [33].

Iron oxide Fe_3O_4 (magnetite) is the main material used in most of these applications, due to its low toxicity, high magnetisation and availability at low cost. In particular, Fe_3O_4 nanoparticles (NPs) are commercially accessible or easy to synthesise, by the co-precipitation method of ferrous and ferric salts under alkaline solution in a controlled N_2 environment, presenting superparamagnetic properties with a saturation magnetisation of ~ 80 Am^2 kg^{-1} [34]. There are several methods to fabricate magnetic alginate materials by physical cross-linking such as, *ex-situ* blending of Fe_3O_4 NPs with the alginate matrix or *in situ* synthesis of Fe_3O_4 NPs in the alginate matrix. The most used method in literature is the blending of alginate and magnetic nanoparticles (MNP), followed by a traditional di-cationic cross-linking protocol [35]. In the second method, *in situ* synthesis of Fe_3O_4 NPs inside of the alginate hydrogel matrix, the alginate hydrogel material is formed by a cross-linking process with ferrous and ferric cations. Then, the material is subjected to a highly alkaline solution and, by diffusion, the Fe_3O_4 NPs are synthesised inside of the material [36].

In biomedical applications using magnetic beads, drug releasing phenomena is achieved over pH ~ 7, since beads swell due to the electrostatic repulsion of the carboxylate groups at this pH [37–38]. Moreover, it has been reported that beads might bust, due to the exchange of the cross-linking cations at that conditions too [39]. On the other hand, a stable and non-degradable hydrogel matrix is in high demand for environmental applications, especially for organic contaminants and heavy metal removal in water resources. In this regard, fundamental understanding of the properties of the nanocomposite obtained when alginate beads are fabricated by both, the *ex situ* and *in situ* processes, is of high

relevance, especially their stability in aqueous medium. In this regards, it is necessary to carry out fundamental studies of the properties and the behaviour of these type of magnetic alginate beads, and to characterise their stability in aqueous medium. Furthermore, it is of special interest to provide to the research community and the biotechnological industry with less complicated synthesis protocols, which overcome the inherent low stability behaviour of magnetic alginate materials.

In this work, magnetic alginate beads (alginate as the polymer matrix and iron oxide as the inorganic matrix) were synthesised using two different methods. First, the direct mix of Fe_3O_4 NP with the alginate solution, *ex situ*, and subsequent gelation with a cationic solution, bead-a, and second, by the *in situ* synthesis of Fe_3O_4 NPs inside of the alginate bead, bead-b. Moreover, in order to improve the stability of the bead-b type, an extra alginate layer was generated on the bead-b by dip coating synthesis, producing bead-c. The stability of the beads was investigated at different pH values and ionic densities in aqueous solution. Moreover, the synthesised magnetic nanoparticles and the beads were characterised by transmission electron microscopy, scanning electron microscopy, X-ray powder diffraction, Fourier-transform infrared, dynamic light scattering, Raman and superconducting quantum interference device in order to understand the behaviour of these magnetic alginate nanocomposites in aqueous solutions.

2. Materials and methods

2.1. Synthesis of the Fe_3O_4 nanoparticles

First, a 0.5 M ferric solution was prepared by dissolving 2.71 g of $FeCl_3 \cdot 6H_2O$ (>99 %, Sigma-Aldrich, Spain) in 20 mL of distilled water and a 0.5 M ferrous solution was prepared by dissolving 1.39 g of $FeSO_4 \cdot 7H_2O$ (>99 %, Sigma-Aldrich, Spain) in 10 mL distilled water. Then, 30 mL Fe^{3+}/Fe^{2+} ($Fe^{3+}:Fe^{2+}$, 2:1) solution (deoxygenated) was added drop by drop in a 40 mL 1 M NaOH (>98 %, Sigma-Aldrich, Spain) solution kept at 40 °C under vigorous stirring and N_2 atmosphere. A black precipitate was immediately formed. Then, the precipitate was heated at 90 °C for 30 min. After that, the precipitate was separated from the solution with a magnet and washed 3 times with distilled water. Finally, the Fe_3O_4 nanoparticles were dried by rotary evaporation at 40 ℃, under vacuum to obtain a black nanoparticle powder [40].

2.2. Synthesis of the alginate beads

Sodium alginate powder (Sigma-Aldrich, Spain), extracted from brown algae with mannuronate (M)/guluronate (G) ratio of ~ 1.56 and molecular weight of 12,000 – 40,000 g mol^{-1}, was used in all synthesised beads.

Bead-a type: 75 mg of Fe_3O_4 NPs were mixed with 5 mL of 1 % (w/v) of sodium alginate solution (1:100, sodium alginate: distilled water). Then, a 15 μL drop of Fe_3O_4/alginate solution was dipped into a 0.1 M calcium chloride (>93 %, Sigma-Aldrich, Spain) solution. The magnetic alginate beads were instantly formed inside of the calcium chloride solution. After 10 min, the beads were removed from the solution and washed with distilled water.

Bead-b type: 15 μL drops of sodium alginate solution were dropped to a 30 mL Fe^{3+} /Fe^{2+} (Fe^{3+}:Fe^{2+}, 2:1) solution (deoxygenated). Yellow coloured beads were formed instantly. The beads were allowed to settle in the solution for 15 min. Then, the beads were washed with distilled water and transferred to a 1 M NaOH solution (deoxygenated) for 10 min to synthesise, *in situ*, the Fe_3O_4 nanoparticles inside of the alginate beads. The yellow colour of the beads instantly turned to black. Finally, the beads were washed with distilled water.

Bead-c type: Beads-b type were dipped into a 0.5 % (w/w) alginate solution and subsequently, transferred to a 0.1 M $CaCl_2$ solution to coat them (10 min) with another alginate layer. Then, the beads were washed with distilled water.

2.3. Characterisation of the nanoparticles and the magnetic beads

Transmission electron microscopy (TEM) images of the Fe_3O_4 nanoparticles (in water suspension) were collected from JEOL JEM 1400 Plus (JEOL, Japan). Scanning electron microscopy (SEM) images of the freeze-dried beads were recorded by Hitachi S-4800 (Hitachi Japan) and QUANTA 200FEG, Field emission scanning electron microscopy (FESEM) for the hydrated beads. Fourier-transform infrared spectroscopy (FTIR) spectra of the dehydrated nanoparticles and beads were carried out, in transmittance mode, using a Jasco 4200 spectrometer. The Raman spectra were recorded by a Renishaw InVia Raman spectrometer, joined to a Leica DMLM microscope. The spectra were acquired with the Leica 50x N Plan (0.75 aperture) objective and 785 nm laser (diode laser, Toptica). X-ray powder diffraction (XRD) patterns were collected by using a Philips X'pert PRO automatic diffractometer operating at 40 kV and 40 mA, in theta-theta configuration, secondary monochromator with Cu-Kα radiation (λ = 1.5418 Å) and a PIXcel solid-state detector (active length in 2θ 3.347 °). Data were collected from 6 to 80° 2θ, step size 0.026 ° and time per step of 450 s at RT (scan speed 0.015 ° s^{-1}). Magnetisation measurements for the iron oxide nanoparticles and the dehydrated beads were carried out in a 5 T Quantum Design MPMS XL-5 (SQUID) magnetometer at room temperature. DLS data were obtained by Malvern Zetasizer Nano-ZS ZEN 3600. Data, statistical and image analysis were carried out in Microsoft Excel, Origin Pro 2018 and Image-J software.

The stability of the beads in aqueous solutions at different pHs was evaluated over time. In order to do that, a pH 2.0 ± 0.2 solution was prepared by diluting HCl (>37 %, Sigma-Aldrich, Spain) and a pH 12.0 ± 0.2 solution was prepared using NaOH (Sigma-Aldrich, Spain). Finally, distilled water was used as the neutral pH solution (pH 7.0 ± 0.5), n = 3. The images of the beads were captured by a Sony Cyber-shot DSC-RX100 camera over time

3. Results and discussion

A schematic illustration of the three types of magnetic alginate beads is presented in Fig. 1. In general, for the three methods, iron oxide alginate nanocomposite liquid suspension or sodium alginate droplets of 15 μL were pipetted into a gelling bath solution containing a Ca^{2+} solution for the bead-a types or into a Fe^{2+} / Fe^{3+} solution for the bead-b types, generating beads of 2.2 ± 0.3 mm diameter (n = 3). The droplets rapidly cross-linked and formed an external outer layer of alginate as a capsule. Then, cations penetrated through the capsule to fully cross-link the alginate polymer to form the bead [41].

3.1. Stability of the beads in aqueous media

Magnetic beads are frequently used for water-based magneto-driven applications. [30] Therefore, it is of great importance to study the stability of the alginate beads in aqueous media, at different pH, over time. In order to do that, the alginate beads were investigated at pH 2.0 ± 0.2, 7.0 ± 0.5 and 12.0 ± 0.2 water solutions up to 21 h. Fig. 2a (left), shows a schematic representation of the behaviour of bead-a at different pH. Bead-a type presented good stability, for all the pH investigated, demonstrating a stable equilibrium, between the water absorption of the bead, over time, and its surrounding medium, as expected for this type of material (n = 3). Alginate beads generally undertake differentiated swelling/ shrinking behaviours in the acidic and in the basic pH solutions. Alginate polymer contains carboxylate groups (–COO^-) which are converted to carboxylic acid (–COOH) in the acidic medium attracting other hydroxyls (–OH) and –COOH groups by intermolecular hydrogen attraction. This effect causes a contraction of the alginate beads over time. On the other hand, at pH values over 7, and especially at basic pH values, the carboxylate groups remain as negative COO^- anions generating electrostatic repulsions forces between the negatively charged groups, expanding the bead resultant to absorb more water molecules and causing the swelling over time until reaching equilibrium [42]. A significant size variation was observed at both pH conditions. The diameter of the beads got reduced by a 16 ± 11 % in the acidic pH = 2.1 medium and increased by a 15 ± 8 % in the basic pH = 12.2 medium (n = 3), see Figure S1.
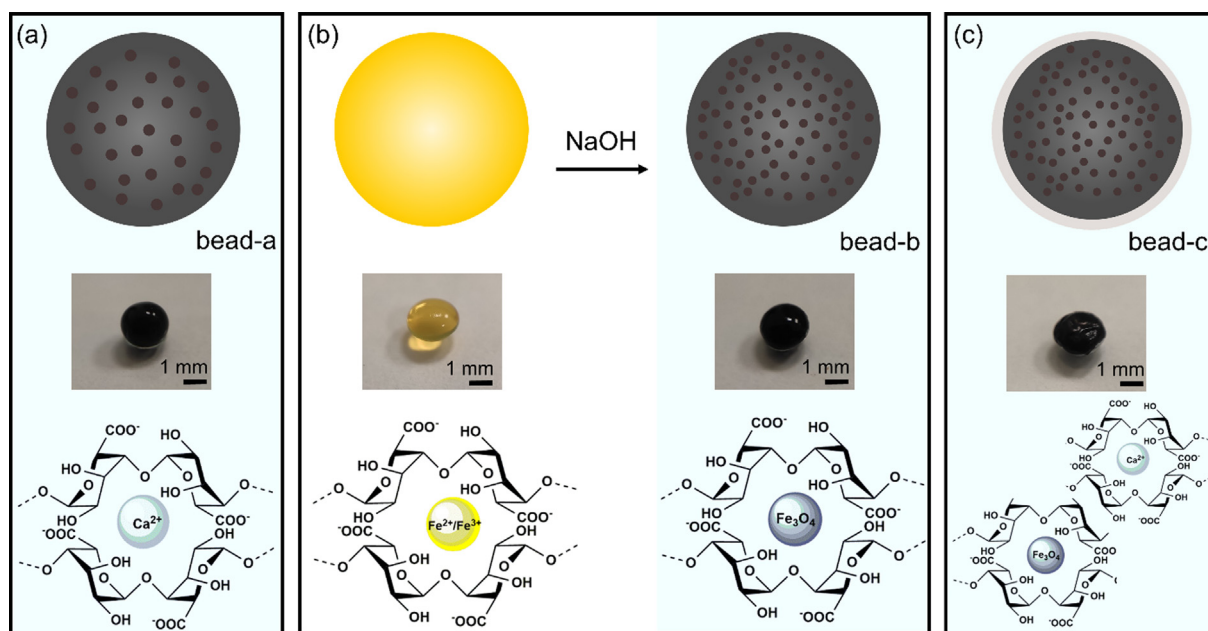
On the other hand, the bead-b type presented a different behaviour compared to bead-a. The beads were found to be stable at high and low pH ranges, obtaining a similar swelling/shrinking behaviour than the bead-a type. However, at neutral pH, the bead-b presented an unstable behaviour, deteriorating rapidly over time, see Fig. 2a schematic diagram (right). This observation is very important to investigate, since neutral pH needs to be used for most of the possible biological applications of these types of beads. The pictures Fig. 2a (right), clearly show that at pH ∼ 7, alginate bead-b rapidly degraded, showing the leaking of the magnetic nanoparticles to the medium. After the first hour, bead-b type was found to swell up to 60 % of its initial size, contributing to the fast degradation of the bead structure and thus, the releasing of the Fe_3O_4 nanoparticles, as a homogeneous suspension, see Figure S2.

This behaviour can be explained considering the instability of the ionic density inside and outside of the beads. In bead-b, the alginate was cross-linked with Fe^{3+} /Fe^{2+} using a ferrous sulphate and ferric chloride solution and then, the Fe_3O_4 nanoparticles were *in situ* synthesised, using a sodium hydroxide solution, inside the beads, as shown by the chemical reaction-1.

$$2FeCl_3 + FeSO_4 + 8NaOH \rightarrow Fe_3O_4 \text{ (NP)} + 6NaCl + Na_2SO_4 + 4H_2O \text{ reaction}$$

(1)
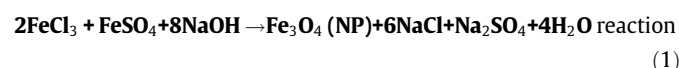
Sodium sulphate and sodium chloride salts remained inside of the alginate beads increasing their internal ionic density. Therefore, when the bead-b is immersed in a neutral pH solution, the bead-b reduced its ionic density by absorbing water molecules, which promoted the rapid swelling of the bead. Besides, the strength of the cross-linked bonds is weaker in the bead-b than in the bead-a, since the nucleation of the Fe_3O_4 nanoparticles decreased the number of available pre-cross-linked bonds. Although, it is expected that the Fe_3O_4 nanoparticles were predominantly formed using the unbounded Fe^{3+} /Fe^{2+} ions present inside of the matrix of the bead, Fe^{3+} /Fe^{2+} ion coming from the cross-linked alginate could get used as well, weakening the stability of the beads at pH ∼ 7. These two effects promoted the fast degradation of the structure of the bead when the osmotic pressure overcome the bond (cross-linking) strength, releasing the magnetic nanoparticles.

U. Bimendra Gunatilake, M. Venkatesan, L. Basabe-Desmonts et al.

Journal of Colloid and Interface Science 610 (2022) 741–750

Fig. 1. Illustration and images of the three types of Fe_3O_4/alginate beads. (a) Bead-a, obtained by direct addition of Fe_3O_4 NPs to the alginate solution, *ex situ*, and subsequent cross-link of the bead in a solution containing Ca^{2+} ions. (b) Bead-b, obtained from an alginate bead cross-linked by Fe^{3+}/Fe^{2+} (yellow bead image) followed by *in situ* synthesis of the Fe_3O_4 nanoparticles inside of the bead (black bead image). (c) Bead-c, obtained from bead-b, followed by the formation of an extra alginate layer cross-linked by a solution of Ca^{2+} ions. The images of the real beads and the chemical illustration for the hydrogels are shown under each bead category.
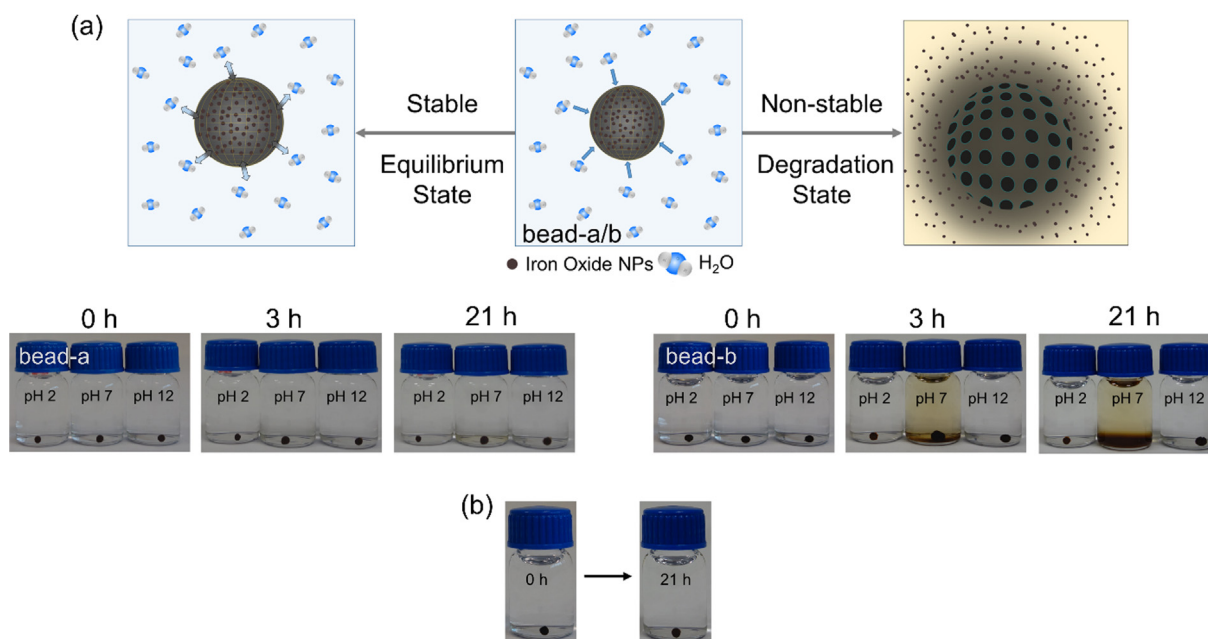
Fig. 2. (a) Schematic illustration of the bead-a and bead-b behaviour at different pH solutions, and pictures of the beads under pH $\sim$ 2, $\sim$7 and $\sim$ 12, from 0 to 21 h. (b) Stability of the bead-b in a NaCl solution (1 M) at pH $\sim$ 7, up to 21 h.

On the other hand, at acidic and basic conditions (pH $\sim$ 2 and $\sim$ 12), the ionic density of the solutions was high, compared to the pH $\sim$ 7 solution thus, water molecules did not rapidly penetrate inside of the bead, reminding in an equilibrium state for longer times.

In order to confirm this behaviour, the magnetic bead-b types were immersed in a solution of 1 M NaCl at neutral pH and monitored over time. Fig. 2b clearly shows that the beads are stable up to 21 h at this high ionic density, confirming that the instability of the ionic density of the inside and the outside of bead is the responsible of the degradation of the bead-b.

Bead-b types have an important advantage compared to bead-a types for the fabrication of magnetic alginate beads. Their simpler synthesis methodology permits the cross-linking of the bead without the inorganic nanoparticles, obtaining higher loadings of the magnetic inorganic material (Fe_3O_4 nanoparticles). Nevertheless, as described above, it has a mayor disadvantage, the low stability and fast degradation of the beads when immersed in a low ionic density medium, becoming an important drawback for most applications. Therefore, in order to overcome this limitation, a third synthesis methodology for the fabrication of magnetic alginate beads was carried out. Bead-c type was synthesised by adding an extra

U. Bimendra Gunatilake, M. Venkatesan, L. Basabe-Desmonts et al.

Journal of Colloid and Interface Science 610 (2022) 741–750

alginate layer cross-linked by calcium divalent ions over the bead-b. Fig. 3a shows the stability of the bead-c at different pH values up to 21 h. Bead-c types are stable in all the pH solutions investigated, preventing the degradation of the beads under low ionic density aqueous media. The extra layer of alginate acts as a protecting shield for the bead-b types. Moreover, during the formation of the extra layer, the diffusion of Ca^{2+} ions reinforced the strength of the entire bead by forming extra cross-linked sides in the bead-b, preventing the breaking of the bead and releasing of the magnetic nanoparticles. As depicted in Fig. 3b, swelling and shrinking behaviour at high and low pH levels, can be clearly seen in bead-c, following the same mechanism mentioned for bead-a. It is remarkable to mention that, larger viability on the diameter of the beads were obtained during the fabrication of the bead-c type, due to the two steps needed for their fabrication.

3.2. Morphological characterisation of the beads

The morphology of the surface and the cross-section of the three bead types were investigated by SEM (from freeze-dried beads) and FESEM (from hydrated beads). Fig. 4a shows the SEM images of the bead-a, bead-b and bead-c surfaces, respectively. Bead-a and bead-c types presented a homogeneously polymerised surface structure without corrosion, which prevented degradation in aqueous environments. On the other hand, a highly porous and corroded surface was observed for the bead-b type. This structure was explained considering that the whole bead, including the surface, contributed to synthesise the Fe_3O_4 nanoparticles inside of the alginate matrix and on the surface of the bead, generating the corroded surface. Further, the morphology of the beads surface was observed by FESEM in their hydrated state. Bead-a presented less porous globular structure, while the bead-b type evidenced an much higher porosity, which facilitated the fast absorption of water and thus, its degradation, see Figure S3. The cross-sectional SEM images of the three beads showed that the porosity is obtained inside of the bead as well, see Fig. 4b. The nucleation of

the magnetic phase in the polymer matrix of the bead-b, modified the cross-linking between –COOH and Fe^{3+} /Fe^{2+}. Therefore, the internal porosity of the bead-b also increased in the same way as its surface porosity. In addition, for bead-c type, the diffusion of extra alginate together with extra cross-linkers, generates a shield layer of calcium alginate, strengthening the bead, as shown in Fig. 4b.

3.3. Morphological characterisation of the magnetic nanoparticles synthesised in the bead-b type

The Fe_3O_4 nanoparticles synthesised inside of the bead-b were fully characterised. They presented a stable suspension in contrast to the conventionally synthesised Fe_3O_4 nanoparticles (nanoparticles used for the magnetic alginate beads-a type). Fig. 5 shows both types of nanoparticles in suspension and after 14 days, and their TEM images. The nanoparticles used for the synthesis of the beads-a aggregated over time due to the dipole–dipole interactions occurring among magnetic nanoparticles [43]. On the other hand, the nanoparticles synthesised inside the bead-b type did not suffer aggregation, presenting a stable nanoparticle suspension in water. Further, high zeta potential of −57.6 mV, in *in situ* synthesised Fe_3O_4 NPs confirmed the stability of the suspension in Fig. 5b, when compared to low zeta potential, −5.79 mV, of Fe_3O_4 NPs used in bead-a. As well, the lower polydispersity index (PDI) value of *in situ* synthesised Fe_3O_4 NPs (0.230) compared to *ex situ* Fe_3O_4 NPs (0.542), convey the increment of monodispersivity in *in situ* Fe_3O_4 NPs; see supplementary information Table S1 for dynamic light scattering data. Moreover, the TEM images confirmed that, the dimensions of the particles synthesised in the bead-b are significantly smaller that the nanoparticles employed for the synthesis of bead-a, being in average ∼ 3 and ∼ 8 nm, respectively. The smaller dimensions of the *in situ* synthesised NPs can be explained considering that the nucleation and the growth of the nanoparticles in bead-b occurred under a pressurised and contracted environment in the polymer matrix, inhibiting their growth.

3.4. Chemical characterisation of the nanoparticles and the beads

3.4.1. XRD analysis
The XRD patterns of the *ex situ* co-precipitated, in bead-a type, and *in situ* synthesised, from bead-b type, nanoparticles were examined in order to check their phase and the iron oxide state. The XRD pattern of the nanoparticles used in bead-a corresponded to magnetite-Fe_3O_4 (JCPDS 75–0449) with main 2θ values at 30.40 °, 35.81 °, 43.38 °, 53.75 °, 57.33 °, 62.93 ° and 18.40 °. On the other hand, the XRD pattern of the nanoparticles synthesised in bead-b matched two XRD data patterns, the magnetite-Fe_3O_4 (JCPDS 88–0315) with 2θ values of 30.40 °, 35.78 °, 43.45 °, 53.88 °, 57.46 ° and 63.064 ° and the sodium chloride (halite crystalline match JCPDS 001–0994) with the 2θ values of 31.87 ° and 45.62 °, see Figure S4a [44–45]. XRD results demonstrated that the magnetite phase of the iron oxide is obtained in both nanoparticles types. In general, in co-precipitated magnetite nanoparticles, the maghemite phase might be presented, which comes from the oxidation of magnetite, this was not clearly appreciated by the XRD analysis, as the X-ray diffraction angles of both maghemite and magnetite are located in the same positions. According to the XRD results, the *in situ* synthesised nanoparticles in bead-b were contaminated with a significant amount of sodium chloride, which is a by-product coming during the synthetic process. Nevertheless, this interference could be removed by performing a hard particle washing step before analysis.

The XRD pattern for the air-dried bead-a and bead-b types matched with the magnetite-Fe_3O_4 (JCPDS 88–0315, JCPDS 75–1609), see Figure S4b. Besides, bead-a type shows an extra phase
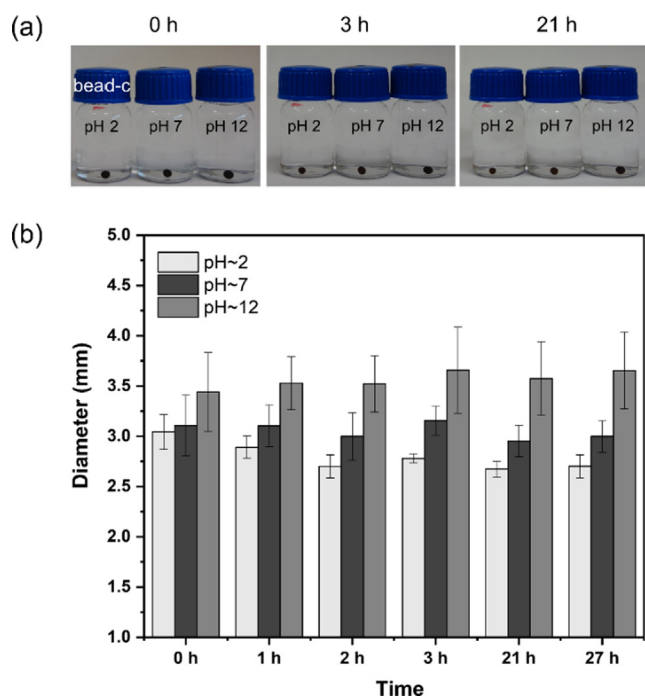

Fig. 3. a) Pictures of the bead-c in aqueous solutions at pH ∼ 2, ∼7 and ∼ 12 for up to 21 h. b) Diameter of the bead-c at the three pH solutions, over time. Sizes were analysed from the images captured by the camera, (n = 3, diameter).
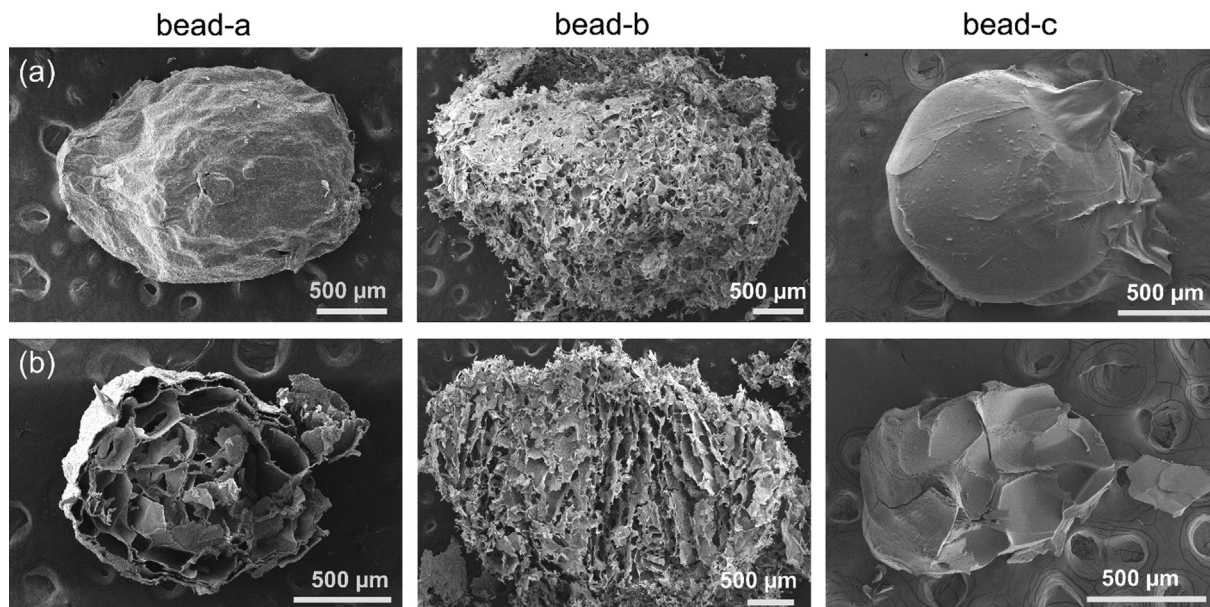
U. Bimendra Gunatilake, M. Venkatesan, L. Basabe-Desmonts et al.

Journal of Colloid and Interface Science 610 (2022) 741–750

Fig. 4. SEM images of freeze-dried beads. Surface images (a) and cross-section images (b) of the three bead types.
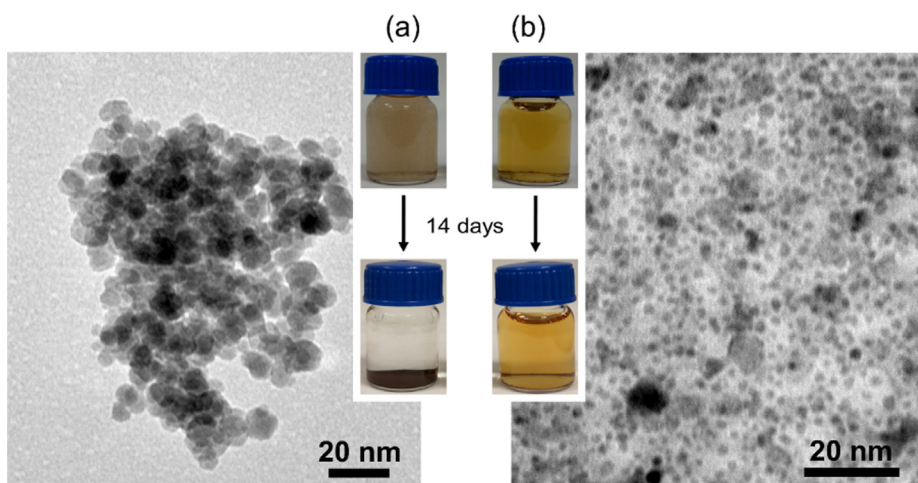

Fig. 5. TEM images of the nanoparticles used in (a) bead-a and (b) *in situ* synthesised in bead-b. Pictures of the dispersed nanoparticles in a bottle when dispersed in water and after 14 days.

at 2θ values of 31.80 ^{o} and 45.55 ^{o} (JCPDS 001–0994) since NaCl formed during the cross-linking process of Na-alginate with $CaCl_2$ in bead-a. In the case of the bead-b type, Na_2SO_4, NaCl and NaOH are bi-products coming from the *in situ* synthesis of the Fe_3O_4 nanoparticles and by the extra diffusion of ions coming from the basic solution. 2θ values at 28.09^{o}, 29.50^{o}, 32.55 ^{o}, 33.91 ^{o} and 38.01 ^{o} can be assigned to Na_2SO_4 (JCPDS 75–0914) while the peaks at 46.30 ^{o} and 55.8 ^{o} (JCPDS 75–0306) and the peaks at 36.99 ^{o}, 40.22 ^{o} and 52.68 ^{o} (JCPDS 01–1173) [44–45] can be assigned to NaCl and NaOH, respectively. These results confirmed that inside the bead-b type there is a significant ionic contamination, contributing to the lower stability of bead-b at neutral pHs, as explained above.

3.4.2. Raman spectra

Raman spectroscopy is able to provide distinguishable identification between magnetite and maghemite phases in synthesised iron oxide nanoparticles, which is usually difficult during XRD analysis. Fe_3O_4 has an inverse spinel type structure, showing five Raman active bands due to the symmetry combination of $A_{1g} + E_g + 3T_{2g}$. [46] In literature, a sharp band at ~ 668 cm^{-1} and two weak bands at ~ 306 and ~ 538 cm^{-1} were observed for A_{1g}, E_g and T_{2g} Raman modes, respectively, for magnetite. On the other hand, for maghemite, a wide band with split peaks at ~ 660 and ~ 710, and ~ 500 cm^{-1} were attributed for A_{1g} and E_g modes, respectively. Furthermore, two high intense red shifted, 306 cm^{-1}, and a blue shifted, 538 cm^{-1} (by magnetite T_{2g}), bands were reported, for magnetite to maghemite oxidation. [47] The Raman spectrum of the Fe_3O_4 nanoparticles used for the synthesis of the bead-a, and the spectrum of the alginate magnetic bead-a were carried out at different laser irradiation powers, Figure S5a and b respectively. The sharp band at 670 cm^{-1} can be attributed to the magnetite A_{1g} mode, while the bands at 490 and 330 cm^{-1} under higher laser power intensity (1.5 mW) were attributed to the oxidation of magnetite to maghemite, in Figure S5a. In literature, the oxidation of magnetite to maghemite has been reported by Ying-Sing Li *et al.* [48] under high laser power irradiations for Fe_3O_4 nanoparticles as the ones used in the synthesis of the

U. Bimendra Gunatilake, M. Venkatesan, L. Basabe-Desmonts et al.

Journal of Colloid and Interface Science 610 (2022) 741–750

bead-a type, confirming this band assignation. The Raman spectra of the bead-a, shown in Figure S5b, at 1.5 mW presented very weak bands at 540 and 307 cm^{-1}, indicating that the oxidation of magnetite to maghemite under high laser power intensities is avoided by the presence of the alginate matrix. The alginate polymer acts as a protective layer for the nanoparticles within the bead-a.

The Raman spectrum of the *in situ* synthesised Fe_3O_4 nanoparticles in bead-b type can be compared to the one of the bare Fe_3O_4 nanoparticles used during the synthesis of the bead-a at 1.5 mW laser power intensity. The absence of the maghemite peaks in *in situ* synthesised Fe_3O_4, according to the Figure S5c, indicates that the *in situ* synthesised Fe_3O_4 were coated with an alginate layer, which avoid the oxidation of *in situ* synthesised Fe_3O_4. Both bead-a and bead-b Raman spectra depicted in Figure S5d, exhibited only the magnetite bands at 670 (sharp), 540 (very weak) and 307 (weak) cm^{-1}, avoiding the oxidation due to the alginate matrix shielding. Moreover, an extra band at 1070 cm^{-1} was observed in the Raman spectra of the bead-b, which was attributed to the sodium sulphate [49], confirming again the high ionic density inside of the bead-b type. The dried beads and *in situ* synthesised Fe_3O_4 nanoparticles did not present any band attributed to maghemite since the nanoparticles were protected with an alginate layer during synthesis process. However, the bare Fe_3O_4 nanoparticles in bead-a have a tendency to oxidize in high (1.5 mW) laser irradiation during the Raman spectra recording.

3.4.3. FTIR spectra

Fig. 6a, shows the FTIR spectra of the two types of magnetic nanoparticles. Similar peaks were obtained for both type of nanoparticles. The bands at 570 and 590 cm^{-1} were attributed to the FeO stretching vibrational bands in tetrahedral and octahedral sites of the Fe_3O_4, while the broad bands at $\sim$ 3400 and $\sim$ 1630 cm^{-1} came from the OH stretching and bending vibrations modes of surface absorbed hydroxyl/water bonds, respectively. Extra bands were observed in the spectrum of the *in situ* synthesised nanoparticles inside the bead-b type. The bands at 1410, 1117 and 1030 cm^{-1} were attributed to the carboxylate COO symmetric stretching vibrations and COC stretching vibrations [46,50]. Moreover, the peak at 1627 cm^{-1} was assigned to the COO asymmetric vibrational band, overlapping with the OH bending vibrations. The presence of these extra peaks demonstrated that the nanoparticles synthesised in the bead-b were coated with an organic alginate layer during nanoparticle nucle-

ation. As explained before, this layer prevented the aggregation of the nanoparticles in the water solution and promoted the formation of smaller, lower nucleation, and more homogeneous distributed nanoparticle suspensions, as presented in Fig. 5b.

Moreover, the FTIR spectra of the two types of beads (bead-a and bead-b) were also performed and compared, Fig. 6b. Considering the peak ascription in the nanoparticle spectra, the bands at 3420/3450, 570/615, 1610/1640, 1405/1445, 1025/1120 cm^{-1} were attributed to the OH stretching, Fe-O stretching, COO asymmetric, COO symmetric and COC stretching vibrational bands, respectively [46].

The difference between band position values (Δv) of asymmetric and symmetric COO stretching vibrational modes provides information about the coordination or the interaction between the inorganic metal phases and the carboxylate groups in alginate polymer matrixes when compared to the Δv of sodium alginate, as demonstrated by Papageorgiou *et al.* [3] According to the Fig. 6b, the calculated values of Δv for bead-a and bead-b are 205 and 195 cm^{-1}, respectively; while the Δv for an Na-alginate was calculated to be 192 cm^{-1}, see Figure S6. Calculated Δv values for calcium alginate and Fe^{3+}/Fe^{2+} alginate are 170 and 179, respectively, Figure S6. In theory, [3,51] when $\Delta v(COO)_{composite} \ll \Delta v(COO)_{alginate}$ the coordination could be considered to be bidentate chelating, $\Delta v(COO)_{composite} \sim \Delta v(COO^-)_{alginate}$ bidentate bridging coordination and unidentate coordination if $\Delta v(COO)_{composite} \gg \Delta v(COO)_{alginate}$. Therefore, considering the Δv values obtained from the different spectra, the addition of Fe_3O_4 nanoparticles to the calcium alginate matrix converted the interaction of bidentate chelating coordination mode to a more unidentate coordination type, which is a stronger egg box model [3]. In the case of the bead-b, bidentate chelating coordination of Fe^{3+}/Fe^{2+} and alginate was converted to bidentate bridging coordination (*in situ* Fe_3O_4 – alginate), after magnetite phase synthesis. In base of the obtained results, it could be speculated that the coordination of the cross-linked metal and the carboxylate group changed after the magnetic phase was introduced into the hydrogel bead-b.

3.5. Magnetic characterisation

The magnetic properties of the synthesised beads (dry state) were characterised by superconducting quantum interference device (SQUID) magnetometer, at room temperature. The magnetisation curves for the synthesised Fe_3O_4 nanoparticles used in bead-

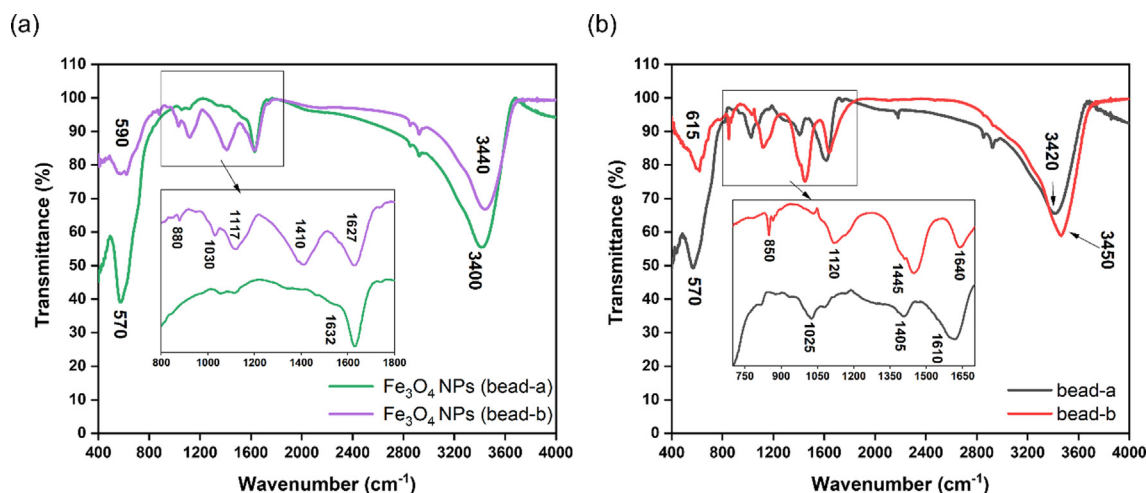**Fig. 6.** (a) FTIR spectra of the nanoparticles used for the synthesis of bead-a (Fe_3O_4 nanoparticles (bead-a)) and the *in situ* synthesised nanoparticles inside the bead-b type (Fe_3O_4 nanoparticles (bead-b)); inset shows the magnified peaks at 800–1800 cm^{-1} range. (b) FTIR spectra of bead-a, and bead-b; inset shows the magnified peaks at 750–1650 cm^{-1} range.

U. Bimendra Gunatilake, M. Venkatesan, L. Basabe-Desmonts et al.

Journal of Colloid and Interface Science 610 (2022) 741–750

a and for the magnetic bead-a, bead-b and bead-c types are presented in the Fig. 7a and b, respectively. The obtained values for the saturation magnetisation (Ms), coercivity (Hc) and remanence (Rm) are depicted in the Table 1.

The Ms value of the bead-a, which contains a 60 % and Fe_3O_4 nanoparticles loading in the alginate, was significantly lower than the expected value, 43.8 Am^2 kg^{-1}, corresponding to Fe_3O_4 nanoparticles (Ms 73.0 Am^2 kg^{-1}) weight ratio during synthesis. The obtained value, 28.2 Am^2 kg^{-1}, can be explained considering the participation of the cross-linkers, Ca^{2+} ions (non-magnetic), in the formation of hydrogel, which caused the reduction of the Ms. Moreover, in this type of hydrogels, a low percentage of magnetic phase loading resulted on the reduction of the magnetisation of the bead in a greater extent, compared to a high percentage of loading, since the participation of none magnetic cross-linkers increases with the alginate percentage. Bead-a exhibited a low or no hysteresis with a very low coercivity and residual magnetisation, close to a superparamagnetic like material, as shown in the inset of Fig. 7a.

The bead-b, which contains the *in situ* synthesised Fe_3O_4 nanoparticles presented a Ms of 41.1 Am^2 kg^{-1}. The magnetic properties of the *in situ* synthesised iron oxide nanoparticles in the bead-b type can be easily manipulated by varying the Fe^{2+}/Fe^{3+} concentrations, the cross-linking concentrations and the diffusing time during the fabrication process. In addition, the smaller size of the magnetic nanoparticles synthesised in the bead-b, resulting in a reduced value of the saturation magnetisation. The extra alginate/Ca^{2+} (non-magnetic) layer to cover the bead-b and generate the bead-c type led to a further reduction of the Ms value, down to 33.5 Am^2 kg^{-1}. Bead-b and bead-c exhibited, as in the case of bead-a, a low or no hysteresis with a very low coercivity and residual magnetisation, reaching to superparamagnetism, see the inset in Fig. 7b. Therefore, considering the flexibility of the fabrication of these types of beads, they could be used for magneto-driven applications.

4. Conclusions

Three different synthesis methods for the fabrication of magnetic alginate beads were carried out and compared. Moreover, the beads were morphologically, chemically and magnetically characterised. Bead-a used the direct blending of Fe_3O_4 nanoparti-

Table 1

Magnetic properties of the Fe_3O_4 nanoparticles used for the synthesis of bead-a, bead-a, bead-b and bead-c.

Sample	Ms (Am^2 kg^{-1})	Hc ($*10^{-3}$ T)	Rm (Am^2 kg^{-1})
Fe_3O_4 nanoparticle (bead-a)	73.0	1.00	0.895
bead-a	28.2	0.96	0.329
bead-b	41.1	1.09	0.870
bead-c	33.5	1.11	0.536

cles (*ex situ*) within an alginate solution, followed by gelation with calcium chloride solution. The bead-b presented the cross-linking of the alginate with a Fe^{3+}/Fe^{2+} solution followed by the *in situ* synthesis of Fe_3O_4 nanoparticles inside of the alginate beads, which is a cheap and efficient protocol to synthesise nanocomposites. Finally, the method-c added an extra alginate layer, cross-linked with calcium ions to the bead-b in order to improve resistance at neutral pH. The stability of the three types of beads was investigated under aqueous solutions at different pH values, over time. It was found that the bead-b type, suffered a fast degradation process at neutral pH, due to the high ionic density inside of the beads.

The *in situ* synthesised nanoparticles, generated in bead-b type, exhibit a low particles size of $\sim$ 3 nm when compared to the Fe_3O_4 nanoparticles used for the synthesis of bead-a ($\sim$8 nm). This was due to the confinement of Fe^{3+}/Fe^{2+} in the alginate hydrogel matrix during the nucleation and growth of the Fe_3O_4 nanoparticles in the bead-b. Moreover, aqueous medium stable suspension of *in situ* synthesised nanoparticles were obtained, with high zeta potential (-57.6 mV), due to the coating of an alginate layer around these particles. In addition, these particles, in bead-b, showed a magnetite crystal phase with a low tendency to oxidise due to the alginate coating. Their magnetisation values, in combination with their low magnetic hysteresis, possibility of using these alginate beads for magneto-driven applications.

This investigation provides with a fundamental framework to understand the properties of blended, *ex situ*, and *in situ* synthesised magnetic metal-oxide based alginate hydrogels. This study will direct the path to select the magnetic bead mode (bead-a, bead-b, bead-c) for different kind of magneto-driven hydrogel applications. Nevertheless, for a particular application of these beads, time-dependent studies longer than 21 h would need to be done in order to characterise for instance, their diffusion prop-
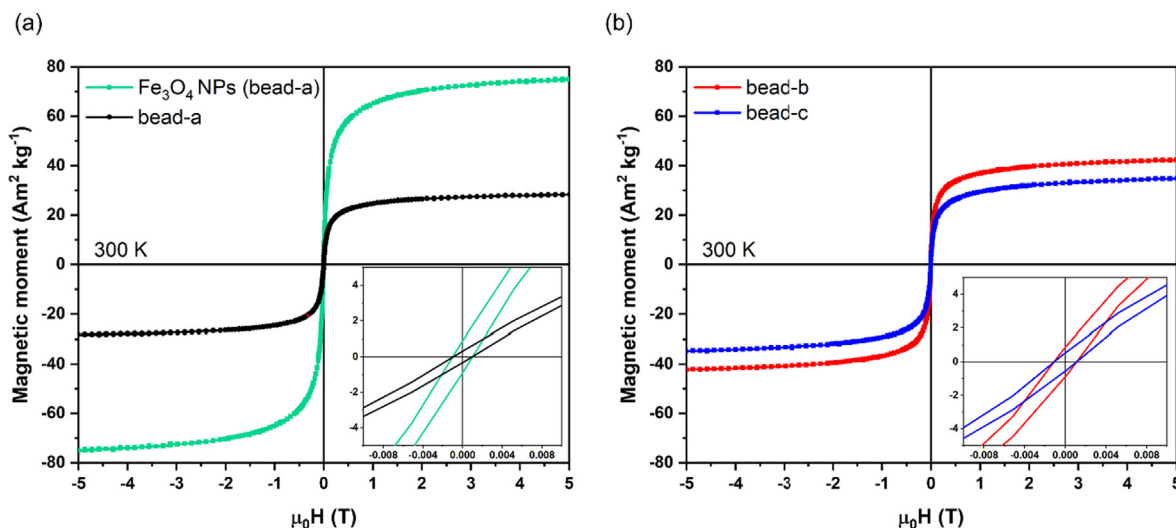
Fig. 7. M-H curves generated by the superconducting quantum interference device (SQUID) magnetometer, at room temperature for: (a) the synthesised iron oxide nanoparticles used in the synthesis of bead-a and of bead-a; (b) bead-b and bead-c. The two insets show the magnification of the graphs around the (0,0) value.

U. Bimendra Gunatilake, M. Venkatesan, L. Basabe-Desmonts et al.

Journal of Colloid and Interface Science 610 (2022) 741–750

erties over time or swelling effects, which could have significant impacts on the performance of the beads.

CRediT authorship contribution statement

Udara Bimendra Gunatilake: Conceptualization, Methodology, Investigation, Writing – original draft, Writing – review & editing. **Munuswamy Venkatesan:** Investigation. **Lourdes Basabe-Desmonts:** Conceptualization, Writing – review & editing, Resources, Supervision, Funding acquisition. **Fernando Benito-Lopez:** Conceptualization, Methodology, Writing – review & editing, Resources, Supervision, Funding acquisition.

Declaration of Competing Interest

The authors declare that they have no known competing financial interests or personal relationships that could have appeared to influence the work reported in this paper.

Acknowledgements

Appendix A. Supplementary material

Supplementary data to this article can be found online at https://doi.org/10.1016/j.jcis.2021.11.119.

References

[1] K.I. Draget, Alginates, Handb. Hydrocoll. Second Ed. (2009) 807–828. https://doi.org/10.1533/9781845695873.807.

[2] B.H.A. Rehm, Alginate Production: Precursor Biosynthesis, Polymerization and Secretion (2009) 55–71, https://doi.org/10.1007/978-3-540-92679-5_2.

[3] S.K. Papageorgiou, E.P. Kouvelos, E.P. Favvas, A.A. Sapalidis, G.E. Romanos, F.K. Katsaros, Metal–carboxylate interactions in metal–alginate complexes studied with FTIR spectroscopy, Carbohydr. Res. 345 (4) (2010) 469–473, https://doi.org/10.1016/j.carres.2009.12.010.

[4] I. Braccini, Serge Pérez, Molecular Basis of Ca2+-Induced Gelation in Alginates and Pectins: The Egg-Box Model Revisited, Biomacromolecules. 2 (2001) 1089–1096, https://doi.org/10.1021/BM010008G.

[5] T. Boontheekul, H.-J. Kong, D.J. Mooney, Controlling alginate gel degradation utilizing partial oxidation and bimodal molecular weight distribution, Biomaterials. 26 (15) (2005) 2455–2465, https://doi.org/10.1016/j.biomaterials.2004.06.044.

[6] B. Sarmento, A. Ribeiro, F. Veiga, P. Sampaio, R. Neufeld, D. Ferreira, Alginate/Chitosan Nanoparticles are Effective for Oral Insulin Delivery, Pharm. Res. 24 (12) (2007) 2198–2206, https://doi.org/10.1007/s11095-007-9367-4.

[7] C. García-Astrain, L. Avérous, Synthesis and evaluation of functional alginate hydrogels based on click chemistry for drug delivery applications, Carbohydr. Polym. 190 (2018) 271–280, https://doi.org/10.1016/J.CARBPOL.2018.02.086.

[8] L.A. Wells, H. Sheardown, Extended release of high pI proteins from alginate microspheres via a novel encapsulation technique, Eur. J. Pharm. Biopharm. 65 (3) (2007) 329–335, https://doi.org/10.1016/j.ejpb.2006.10.018.

[9] J. Park, S.J. Lee, H. Lee, S.A. Park, J.Y. Lee, Three dimensional cell printing with sulfated alginate for improved bone morphogenetic protein-2 delivery and osteogenesis in bone tissue engineering, Carbohydr. Polym. 196 (2018) 217–224, https://doi.org/10.1016/J.CARBPOL.2018.05.048.

[10] W. E, K. D, Alginate matrices for protein delivery - a short review, Physiol. Res. 67 (2018) s319–s334. https://doi.org/10.33549/PHYSIOLRES.933980.

[11] R. Ma, Y. Wang, H. Qi, C. Shi, G. Wei, L. Xiao, Z. Huang, S. Liu, H. Yu, C. Teng, H. Liu, V. Murugadoss, J. Zhang, Y. Wang, Z. Guo, Nanocomposite sponges of sodium alginate/graphene oxide/polyvinyl alcohol as potential wound dressing: In vitro and in vivo evaluation, Compos. Part B Eng. 167 (2019) 396–405, https://doi.org/10.1016/J.COMPOSITESB.2019.03.006.

[12] B.A. Aderibigbe, B. Buyana, Alginate in Wound Dressings, Pharm. 2018, Vol. 10, Page 42. 10 (2018) 42. https://doi.org/10.3390/PHARMACEUTICS10020042.

[13] P.S.P. Batista, A.M.M.B. de Morais, M.M.E. Pintado, R.M.S.C. de Morais, Alginate: Pharmaceutical and Medical Applications, (2019) 649–691. https://doi.org/10.1007/978-3-030-12919-4_16

[14] Mariam Mir, Murtaza Najabat Ali, Afifa Barakullah, Ayesha Gulzar, Munam Arshad, Shizza Fatima, Maliha Asad, Synthetic polymeric biomaterials for wound healing: a review, Prog. Biomater. 7 (1) (2018) 1–21, https://doi.org/10.1007/s40204-018-0083-4.

[15] C.K. Kuo, P.X. Ma, Ionically crosslinked alginate hydrogels as scaffolds for tissue engineering: Part 1. Structure, gelation rate and mechanical properties, Biomaterials 22 (6) (2001) 511–521, https://doi.org/10.1016/S0142-9612(00)00201-5.

[16] N. Contessi Negrini, M. Bonnetier, G. Giatsidis, D.P. Orgill, S. Farè, B. Marelli, Tissue-mimicking gelatin scaffolds by alginate sacrificial templates for adipose tissue engineering, Acta Biomater. 87 (2019) 61–75, https://doi.org/10.1016/J.ACTBIO.2019.01.018.

[17] K. Álvarez, V.A. Alvarez, T.J. Gutiérrez, Biopolymer Composite Materials with Antimicrobial Effects Applied to the Food Industry, (2018) 57–96. https://doi.org/10.1007/978-3-319-66417-0_3.

[18] Y. Qin, J. Jiang, L. Zhao, J. Zhang, F. Wang, Applications of Alginate as a Functional Food Ingredient, Biopolym. Food Des. (2018) 409–429, https://doi.org/10.1016/B978-0-12-811449-0.00013-X.

[19] S. Thakur, B. Sharma, A. Verma, J. Chaudhary, S. Tamulevicius, V.K. Thakur, Recent progress in sodium alginate based sustainable hydrogels for environmental applications, J. Clean. Prod. 198 (2018) 143–159, https://doi.org/10.1016/J.JCLEPRO.2018.06.259.

[20] Yuan Zhuang, Yan Kong, Xuechun Wang, Baoyou Shi, Novel one step preparation of a 3D alginate based MOF hydrogel for water treatment, New J. Chem. 43 (19) (2019) 7202–7208, https://doi.org/10.1039/C8NJ06031B.

[21] N. Peng, X. Ding, Z. Wang, Y. Cheng, Z. Gong, X. Xu, X. Gao, Q. Cai, S. Huang, Y. Liu, Novel dual responsive alginate-based magnetic nanogels for onco-theranostics, Carbohydr. Polym. 204 (2019) 32–41, https://doi.org/10.1016/J.CARBPOL.2018.09.084.

[22] P.M. Tamhankar, A.M. Kulkarni, S.C. Watawe, P.M. Tamhankar, A.M. Kulkarni, S.C. Watawe, Functionalization of Cobalt Ferrite Nanoparticles with Alginate Coating for Biocompatible Applications, Mater. Sci. Appl. 2 (2011) 1317–1321, https://doi.org/10.4236/MSA.2011.29179.

[23] Priscilla Vanessa Finotelli, Daniel Da Silva, Mauro Sola-Penna, Alexandre Malta Rossi, Marcos Farina, Leonardo Rodrigues Andrade, Armando Yoshihaki Takeuchi, Maria Helena Rocha-Leão, Microcapsules of alginate/chitosan containing magnetic nanoparticles for controlled release of insulin, Colloids Surfaces B Biointerfaces. 81 (1) (2010) 206–211, https://doi.org/10.1016/j.colsurfb.2010.07.008.

[24] Annette M. Schmidt, Thermoresponsive magnetic colloids, Colloid Polym. Sci. 285 (9) (2007) 953–966, https://doi.org/10.1007/s00396-007-1667-z.

[25] S. Kondaveeti, A.T.S. Semeano, D.R. Cornejo, H. Ulrich, D.F.S. Petri, Magnetic hydrogels for levodopa release and cell stimulation triggered by external magnetic field, Colloids Surfaces B Biointerfaces. 167 (2018) 415–424, https://doi.org/10.1016/J.COLSURFB.2018.04.040.

[26] Tetsu Mitsumata, Yusuke Kakiuchi, Jun-Ichi Takimoto, Fast drug release using rotational motion of magnetic gel beads, Res. Lett. Phys. Chem. 2008 (2008) 1–5, https://doi.org/10.1155/2008/671642.

[27] C.H. Yang, C.C. Yen, J.J. Jheng, C.Y. Wang, S.S. Chen, P.Y. Huang, K.S. Huang, J.F. Shaw, Immobilization of Brassica oleracea chlorophyllase 1 (BoCLH1) and Candida rugosa lipase (CRL) in magnetic alginate beads: An enzymatic evaluation in the corresponding proteins, Molecules 19 (8) (2014) 11800–11815, https://doi.org/10.3390/MOLECULES190811800.

[28] Séverine Brulé, Michael Levy, Claire Wilhelm, Didier Letourneur, Florence Gazeau, Christine Ménager, Catherine Le Visage, Doxorubicin Release Triggered by Alginate Embedded Magnetic Nanoheaters: A Combined Therapy, Adv. Mater. 23 (6) (2011) 787–790, https://doi.org/10.1002/adma.201003763.

[29] M. Amiri, M. Salavati-Niasari, A. Pardakhty, M. Ahmadi, A. Akbari, Caffeine: A novel green precursor for synthesis of magnetic CoFe2O4 nanoparticles and pH-sensitive magnetic alginate beads for drug delivery, Mater. Sci. Eng. C. 76 (2017) 1085–1093, https://doi.org/10.1016/J.MSEC.2017.03.208.

[30] Vincent Rocher, Jean-Michel Siaugue, Valérie Cabuil, Agnès Bee, Removal of organic dyes by magnetic alginate beads, Water Res. 42 (4-5) (2008) 1290–1298, https://doi.org/10.1016/j.watres.2007.09.024.

[31] Zhimin Lei, Shangru Zhai, Jialiang Lv, Yuan Fan, Qingda An, Zuoyi Xiao, Sodium alginate-based magnetic carbonaceous biosorbents for highly efficient Cr(vi) removal from water, RSC Adv. 5 (2015) 77932–77941, https://doi.org/10.1039/C5RA13226F.

[32] Agnès Bée, Delphine Talbot, Sébastien Abramson, Vincent Dupuis, Magnetic alginate beads for Pb(II) ions removal from wastewater, J. Colloid Interface Sci. 362 (2) (2011) 486–492, https://doi.org/10.1016/j.jcis.2011.06.036.

[33] Yanting Liu, Yuanyuan Yang, Xiong Yang, Liu Yang, Yajing Shen, Wanfeng Shang, Multi-functionalized micro-helical capsule robots with superior loading and releasing capabilities, J. Mater. Chem. B. 9 (5) (2021) 1441–1451, https://doi.org/10.1039/D0TB02329A.

[34] Olga Philippova, Anna Barabanova, Vyacheslav Molchanov, Alexei Khokhlov, Magnetic polymer beads: Recent trends and developments in synthetic design

and applications, Eur. Polym. J. 47 (4) (2011) 542–559, https://doi.org/10.1016/j.eurpolymj.2010.11.006.

[35] Samia Ben Hammouda, Nafaâ Adhoum, Lotfi Monser, Synthesis of magnetic alginate beads based on Fe3O4 nanoparticles for the removal of 3-methylindole from aqueous solution using Fenton process, J. Hazard. Mater. 294 (2015) 128–136, https://doi.org/10.1016/j.jhazmat.2015.03.068.

[36] A. Soumia, M. Adel, S. Amina, B. Bouhadjar, D. Amal, Z. Farouk, B. Abdelkader, S. Mohamed, Fe3O4-alginate nanocomposite hydrogel beads material: One-pot preparation, release kinetics and antibacterial activity, Int. J. Biol. Macromol. 145 (2020) 466–475, https://doi.org/10.1016/J.IJBIOMAC.2019.12.211.

[37] B. Rashidzadeh, E. Shokri, G.R. Mahdavinia, R. Moradi, S. Mohamadi-Aghdam, S. Abdi, Preparation and characterization of antibacterial magnetic-/pH-sensitive alginate/Ag/Fe3O4 hydrogel beads for controlled drug release, Int. J. Biol. Macromol. 154 (2020) 134–141, https://doi.org/10.1016/J.IJBIOMAC.2020.03.028.

[38] Fa-Qin Wang, Ping Li, Jun-Ping Zhang, Ai-Qin Wang, Qin Wei, A novel pH-sensitive magnetic alginate-chitosan beads for albendazole delivery, Drug Dev. Ind. Pharm. 36 (7) (2010) 867–877, https://doi.org/10.3109/03639040903567117.

[39] J. Supramaniam, R. Adnan, N.H. Mohd Kaus, R. Bushra, Magnetic nanocellulose alginate hydrogel beads as potential drug delivery system, Int. J. Biol. Macromol. 118 (2018) 640–648, https://doi.org/10.1016/J.IJBIOMAC.2018.06.043.

[40] Sophie Laurent, Delphine Forge, Marc Port, Alain Roch, Caroline Robic, Luce Vander Elst, Robert N. Muller, Magnetic Iron Oxide Nanoparticles: Synthesis, Stabilization, Vectorization, Physicochemical Characterizations, and Biological Applications, Chem. Rev. 108 (6) (2008) 2064–2110, https://doi.org/10.1021/cr068445e.

[41] J.Y. Leong, W.H. Lam, K.W. Ho, W.P. Voo, M.F.X. Lee, H.P. Lim, S.L. Lim, B.T. Tey, D. Poncelet, E.S. Chan, Advances in fabricating spherical alginate hydrogels with controlled particle designs by ionotropic gelation as encapsulation systems, Particuology. 24 (2016) 44–60, https://doi.org/10.1016/J.PARTIC.2015.09.004.

[42] S.K. Bajpai, Shubhra Sharma, Investigation of swelling/degradation behaviour of alginate beads crosslinked with Ca2+ and Ba2+ ions, React. Funct. Polym. 59 (2) (2004) 129–140, https://doi.org/10.1016/j.reactfunctpolym.2004.01.002.

[43] Lucía Gutiérrez, Leonor de la Cueva, María Moros, Eva Mazarío, Sara de Bernardo, Jesús M de la Fuente, M Puerto Morales, Gorka Salas, Aggregation effects on the magnetic properties of iron oxide colloids, Nanotechnology. 30 (11) (2019) 112001, https://doi.org/10.1088/1361-6528/aafbff.

[44] Stacy Gates-Rector, Thomas Blanton, The Powder Diffraction File: a quality materials characterization database, Powder Diffr. 34 (4) (2019) 352–360, https://doi.org/10.1017/S0885715619000812.

[45] Saulius Gražulis, Daniel Chateigner, Robert T. Downs, A.F.T. Yokochi, Miguel Quirós, Luca Lutterotti, Elena Manakova, Justas Butkus, Peter Moeck, Armel Le Bail, Crystallography Open Database - an open-access collection of crystal structures, J. Appl. Crystallogr. 42 (4) (2009) 726–729, https://doi.org/10.1107/S0021889809016690.

[46] Manish Srivastava, Jay Singh, Madhu Yashpal, Dinesh Kumar Gupta, R.K. Mishra, Shipra Tripathi, Animesh K. Ojha, Synthesis of superparamagnetic bare Fe3O4 nanostructures and core/shell (Fe3O4/alginate) nanocomposites, Carbohydr. Polym. 89 (3) (2012) 821–829, https://doi.org/10.1016/j.carbpol.2012.04.016.

[47] S.P. Schwaminger, D. Bauer, P. Fraga-García, F.E. Wagner, S. Berensmeier, Oxidation of magnetite nanoparticles: impact on surface and crystal properties, CrystEngComm. 19 (2) (2017) 246–255, https://doi.org/10.1039/C6CE02421A.

[48] Ying-Sing Li, Jeffrey S. Church, Andrea L. Woodhead, Infrared and Raman spectroscopic studies on iron oxide magnetic nano-particles and their surface modifications, J. Magn. Magn. Mater. 324 (8) (2012) 1543–1550, https://doi.org/10.1016/j.jmmm.2011.11.065.

[49] Kawther Ben Mabrouk, Thomas H. Kauffmann, Hassen Aroui, Marc D. Fontana, Raman study of cation effect on sulfate vibration modes in solid state and in aqueous solutions, J. Raman Spectrosc. 44 (11) (2013) 1603–1608, https://doi.org/10.1002/jrs.4374.

[50] A. Mohammadi, H. Daemi, M. Barikani, Fast removal of malachite green dye using novel superparamagnetic sodium alginate-coated Fe3O4 nanoparticles, Int. J. Biol. Macromol. 69 (2014) 447–455, https://doi.org/10.1016/J.IJBIOMAC.2014.05.042.

[51] K. Nakamoto, Infrared and Raman Spectra of Inorganic and Coordination Compounds, Handb. Vib. Spectrosc. (2006), https://doi.org/10.1002/0470027320.S4104.